Generalized Graph-Based Fusion of Hyperspectral and LiDAR Data Using Morphological Features

Wenzhi Liao, *Member, IEEE*, Aleksandra Pižurica, *Member, IEEE*, Rik Bellens, Sidharta Gautama, and Wilfried Philips, *Senior Member, IEEE*

***Abstract*—Nowadays, we have diverse sensor technologies and image processing algorithms that allow one to measure different aspects of objects on the Earth [e.g., spectral characteristics in hyperspectral images (HSIs), height in light detection and ranging (LiDAR) data, and geometry in image processing technologies, such as morphological profiles (MPs)]. It is clear that no single technology can be sufficient for a reliable classification, but combining many of them can lead to problems such as the curse of dimensionality, excessive computation time, and so on. Applying feature reduction techniques on all the features together is not good either, because it does not take into account the differences in structure of the feature spaces. Decision fusion, on the other hand, has difficulties with modeling correlations between the different data sources. In this letter, we propose a *generalized* graph-based fusion method to couple dimension reduction and feature fusion of the spectral information (of the original HSI) and MPs (built on both HS and LiDAR data). In the proposed method, the edges of the fusion graph are weighted by the distance between the stacked feature points. This yields a clear improvement over an older approach with binary edges in the fusion graph. Experimental results on real HSI and LiDAR data demonstrate effectiveness of the proposed method both visually and quantitatively.**

***Index Terms*—Data fusion, graph-based, hyperspectral image (HSI), light detection and ranging (LiDAR) data, remote sensing.**

I. Introduction

RECENT advances in the remote sensing technology have led to an increased availability of multisensor data from the same area. In particular, hyperspectral images (HSIs) provide a detailed description of the spectral signatures of ground covers, whereas light detection and ranging (LiDAR) data give detailed information about the height of the same surveyed area. The HS data, once combined with LiDAR data, can provide a more comprehensive interpretation of objects on the ground. Many techniques have been developed for fusion of HS and LiDAR data in a classification task [1]–[6]. Simental *et al.* [1] explored the joint use of HS and LiDAR data for the separation of vegetation classes, underlining that LiDAR can be very useful in the separation of shrubs from trees. Lemp and Weidner [2] exploited HS and LiDAR data for the classification of urban areas, using LiDAR for the segmentation of the scene and then HS data for the classification of the resulting regions. Koetz *et al.* [3] classified fuel composition from fused LiDAR and HS bands using support vector machines (SVMs) and showed that the classification accuracies after fusion were higher than those based on either sensor alone. Multiple feature fusion using decision fusion and manifold learning were proposed for classification of HS remote sensing imagery in [7] and [8]. Huang *et al.* [4] compared vector stacking, reclassification, and postprocessing for information fusion of aerial images and LiDAR data in urban areas. The joint use of HS and LiDAR remote sensing data for the classification of complex forest areas was investigated in [5]. They proposed a novel classification system based on different possible classifiers that were able to properly integrate multisensor information. Recently, Pedergnana *et al.* [6] have applied morphological extended attribute profiles (EAPs) [9] to both HS and LiDAR data for a classification task. Their method jointly considered the features extracted by EAPs computed on both HS and LiDAR data and fused spectral, spatial, and elevation information in a stacked architecture.

Despite the simplicity of such feature fusion methods (that simply concatenate several kinds of feature sources), the systems do not always perform better (and can even perform worse) than using a single feature source. Dalla Mura *et al.* [10] showed examples where the classification accuracies by stacking different morphological attributes were even lower than by using only single morphological attribute. This is because the information contained in different feature sources is not well represented or measured. Furthermore, the resulting data by stacking several kinds of feature sources may contain redundant information. Last, but not least, the increase in the dimensionality of the stacked features, as well as the limited number of labeled samples in many real applications, may pose the problem of the curse of dimensionality and, as a consequence, result in the risk of overfitting the training data.

An older version of our graph-based data fusion method with binary edges of the fusion graph won the "Best Paper Challenge" Award at the 2013 IEEE Data Fusion Contest [11]. In this letter, we propose a *generalized* graph-based fusion of HS and LiDAR (GGF). An important difference with [11] is that the proposed fusion graph does not simply set the edges of fusion graph to 0 (disconnected) or 1 (connected) but employs *weighted* edges (with weights corresponding to the distance between the stacked feature points). In this way, we build a more general weighted fusion graph where the actual

Manuscript received May 27, 2014; revised July 29, 2014; accepted August 14, 2014. This work was supported by the SBO-IWT project Chameleon: Domain-specific Hyperspectral Imaging Systems for Relevant Industrial Applications.

The authors are with the Image Processing and Interpretation, Department of Telecommunications and Information Processing, iMinds, Ghent University, 9000 Ghent, Belgium (e-mail: Wenzhi.Liao@telin.ugent.be; Aleksandra.Pizurica@telin.ugent.be; Rik.Bellens@telin.ugent.be; Sidharta.Gautama@telin.ugent.be; Wilfried.Philips@telin.ugent.be).

Color versions of one or more of the figures in this paper are available online at http://ieeexplore.ieee.org.

Digital Object Identifier 10.1109/LGRS.2014.2350263

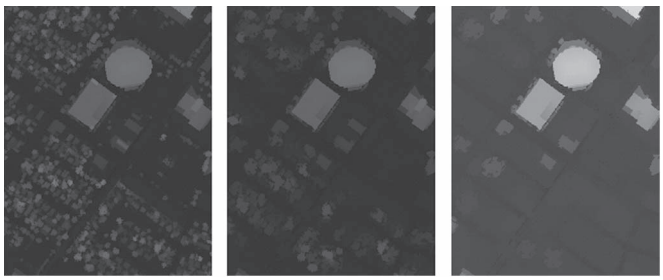

Fig. 1. Openings on a part of LiDAR data with disk-shaped SEs of increasing radius size (1, 3, and 5).

differences and similarities in spectral, spatial, and elevation characteristics of the feature points are better modeled. The proposed fusion graph is hence more general and more powerful than the binary one. The organization of this letter is as follows. Section II provides a brief review of morphological features. In Section III, we present the proposed graph-based feature fusion method. The experimental results on real urban HSIs are presented and discussed in Section IV. Finally, the conclusions are drawn in Section V.

II. Morphological Features

Morphological features are generated by applying either morphological openings or closings by reconstruction on the image, using a structural element (SE) of predefined size and shape. For example, the morphological profile (MP) with a disk SE carries information about the minimum size of objects, whereas the directional MP indicates the maximum size of objects [12]–[14]. An opening acts on bright objects (areas with high elevation in LiDAR data, such as the top of the roof) compared with their surrounding, whereas closings act on dark (low height in the LiDAR data) objects. For example, an opening deletes bright objects that are smaller than the SE.[1] By increasing the size of the SE and repeating the previous operation, a complete MP is built, carrying information about the size and the shape of objects in the image.

In our experiments, morphological features are generated by applying morphological openings and closings with partial reconstruction [12]–[14] on both LiDAR data and the first two principal components (PCs) (representing more than 99% of the cumulative variance) of the original HSI. For a disk-shaped SE, MPs with 15 openings and closings (ranging from 1 to 15 with a step-size increment of 1) are computed for both LiDAR data and the first two PCs of the HSI. For linear structuring elements, we take the maximum (for openings) or minimum (for closings) over multiple orientations (every 10°) and use 10% of the length of the SE for partial reconstruction. Then, we generate MPs with 20 openings and closings (ranging from 5 to 100 with a step-size increment of 5) for both LiDAR data and the first two PCs of the HSI. Fig. 1 shows the results of the MP with partial reconstruction for LiDAR data with different scales. As the size of the SE increases in openings, we can see that more and more bright objects (i.e., objects with high elevation) disappear in the dark background of LiDAR data. The effect of using disk- and linear-based morphological features with partial reconstruction for classification of remote sensing data from urban areas has been discussed in our previous work [12]–[14].

[1]Deleting means here that the pixels in the object take on the value of their surrounding.

III. Proposed Fusion Method

Different feature sources typically have a different range of values, different dimensions, and different characteristics. For example, an original HSI with 144 bands contains the spectral information of the ground covers. The morphological features of LiDAR data with 70 bands (with 30 bands of disk-based MPs and 40 bands of directional MPs) carry the elevation information of the same surveyed area. The morphological features obtained from the HSI have 140 bands and carry the spatial information. Before fusing all the feature sources, we normalize their dimensions and reduce the noise throughout the given feature space with kernel principal component analysis (KPCA) [14], [15], like we also did in [11]. We assume that the dimension of each feature source is already normalized to the smallest dimension of all the feature sources $D = 70$. Let $\mathbf{X}^{\mathrm{Spe}} = \{\mathbf{x}_i^{\mathrm{Spe}}\}_{i=1}^n$, $\mathbf{X}^{\mathrm{Spa}} = \{\mathbf{x}_i^{\mathrm{Spa}}\}_{i=1}^n$, and $\mathbf{X}^{\mathrm{Ele}} = \{\mathbf{x}_i^{\mathrm{Ele}}\}_{i=1}^n$ denote the spectral, spatial (the spatial features are obtained from the HS data), and elevation features, respectively, where $\mathbf{x}_i^{\mathrm{Spe}} \in \mathbb{R}^D$, $\mathbf{x}_i^{\mathrm{Spa}} \in \mathbb{R}^D$, and $\mathbf{x}_i^{\mathrm{Ele}} \in \mathbb{R}^D$ after normalization to the same dimension. $\mathbf{X}^{\mathrm{Sta}} = \{\mathbf{x}_i^{\mathrm{Sta}}\}_{i=1}^n = [\mathbf{X}^{\mathrm{Spe}}; \mathbf{X}^{\mathrm{Spa}}; \mathbf{X}^{\mathrm{Ele}}]$, and $\mathbf{x}_i^{\mathrm{Sta}} = [\mathbf{x}_i^{\mathrm{Spe}}; \mathbf{x}_i^{\mathrm{Spa}}; \mathbf{x}_i^{\mathrm{Ele}}] \in \mathbb{R}^{3D}$ denotes the vector stacked by the spectral, spatial, and altitude features. $\{\mathbf{z}_i\}_{i=1}^n$, and $\mathbf{z}_i \in \mathbb{R}^d$ denote the fusion features in a lower dimensional feature space with $d \leq 3D$.

The goal of this letter is to find a transformation matrix $\mathbf{W} \in \mathbb{R}^{3D \times d}$, which can couple dimensionality reduction and feature fusion in a way of $\mathbf{z}_i = \mathbf{W}^T \mathbf{x}_i$ ($\mathbf{x}_i$ is a variable, which can be set to be $\mathbf{x}_i^{\mathrm{Sta}}$, $\mathbf{x}_i^{\mathrm{Spe}}$, etc.). The transformation matrix $\mathbf{W}$ should not only fuse different features in a lower dimensional feature space but also preserve local neighborhood information and detect the manifold embedded in the high-dimensional feature space. A reasonable way [16] to find the transformation matrix $\mathbf{W}$ can be defined as follows:

$$\arg \min_{\mathbf{W} \in \mathbb{R}^{3D \times d}} \left(\sum_{i,j=1}^{n} \|\mathbf{W}^T \mathbf{x}_i - \mathbf{W}^T \mathbf{x}_j\|^2 A_{ij} \right) \tag{1}$$

where the matrix $\mathbf{A}$ is the edge of the graph $\mathbf{G} = (\mathbf{X}, \mathbf{A})$.

In our previous work [11], we assumed that the edges (between data points $\mathbf{x}_i$ and $\mathbf{x}_j$) are binary, i.e., $A_{ij} \in \{0, 1\}$. $A_{ij} = 1$ if $\mathbf{x}_i$ and $\mathbf{x}_j$ are "close," and $A_{ij} = 0$ if $\mathbf{x}_i$ and $\mathbf{x}_j$ are "far apart." "Close" was defined by finding the k-nearest neighbors (k-NN) of the data point $\mathbf{x}_i$. The k-NN is determined first by calculating the Euclidean distance between data point $\mathbf{x}_i$ and all the data points, then sorting the distance and determining the nearest neighbors based on the kth minimum distance. A fusion graph $\mathbf{G}^{\mathrm{Fus}} = (\mathbf{X}^{\mathrm{Sta}}, \mathbf{A}^{\mathrm{Fus}})$ was defined as follows:

$$\mathbf{A}^{\mathrm{Fus}} = \mathbf{A}^{\mathrm{Spe}} \odot \mathbf{A}^{\mathrm{Spa}} \odot \mathbf{A}^{\mathrm{Ele}} \tag{2}$$

with "$\odot$" denoting element-wise multiplication, i.e., $A_{i,j}^{\mathrm{Fus}} = A_{i,j}^{\mathrm{Spe}} A_{i,j}^{\mathrm{Spa}} A_{i,j}^{\mathrm{Ele}}$, and $A_{ij}^{\mathrm{Fus}} = 1$ only if $A_{ij}^{\mathrm{Spe}} = 1$, $A_{ij}^{\mathrm{Spa}} = 1$,

TABLE I
CLASSIFICATION ACCURACIES OBTAINED BY THE DESCRIBED SCHEMES

	Raw$_{HS}$	MPs$_{HS}$	MPs$_{Li}$	MPs$_{HSLi}$	Sta	PCA	NWFE	LPP	GFHL$_{org}$	GGF$_{org}$	GFHL	GGF
Number of Features	144	140	70	210	210	35	42	26	36	28	24	22
OA (%)	80.72	82.43	69.39	86.39	87.49	85.28	87.96	90.74	88.59	91.28	93.29	**94.0**
AA (%)	83.40	84.99	68.42	88.48	88.94	87.29	88.88	91.26	89.43	91.24	93.19	**93.79**
κ	0.792	0.810	0.668	0.853	0.864	0.840	0.869	0.900	0.876	0.903	0.927	**0.935**
Consumed Time (s)	238.3	230.9	163.9	258.9	1159.4	88.1	1338.2	655.7	131.3	83.4	628.8	629.6
(#198 / #1053) Grass Healthy	82.15	80.25	35.61	82.43	81.10	78.63	81.29	**82.91**	82.72	82.53	82.24	**82.91**
(#190 / #1064) Grass Stressed	81.58	80.64	67.11	82.61	84.87	81.77	83.27	87.41	84.96	98.68	88.91	**99.34**
(#192 / #505) Grass Synthetis	99.80	**100**	79.60	**100**	**100**	**100**	**100**	**100**	**100**	**100**	**100**	**100**
(#188 / #1056) Tree	92.80	84.09	72.92	91.10	95.45	93.75	89.49	98.86	97.73	98.96	99.24	**99.34**
(#186 / #1056) Soil	97.92	**100**	83.52	99.91	99.91	99.91	99.81	99.91	99.15	**100**	**100**	**100**
(#182 / #143) Water	95.10	95.10	66.43	**100**	95.80	95.80	95.80	95.10	95.80	95.10	95.10	95.10
(#196 / #1072) Residential	76.21	87.31	76.59	80.97	86.94	84.70	86.38	**92.28**	87.22	90.95	89.18	90.86
(#191 / #1053) Commercial	54.51	45.58	91.03	63.06	59.54	66.95	76.07	86.23	85.38	90.98	95.54	**95.63**
(#193 / #1059) Road	78.47	91.03	59.21	91.88	90.37	83.66	**93.58**	91.88	89.80	90.46	91.03	89.33
(#191 / #1036) Highway	60.04	60.42	64.86	64.67	65.44	57.53	62.16	72.97	66.89	60.91	**98.65**	92.76
(#181 / #1054) Railway	79.51	87.10	88.24	93.45	**99.24**	97.34	98.39	96.87	98.20	94.46	97.34	96.58
(#192 / #1041) Parking Lot 1	82.90	86.84	70.89	97.89	99.33	91.74	**99.90**	90.2	84.62	99.14	88.95	91.93
(#184 / #285) Parking Lot 2	72.63	76.49	55.09	**79.30**	77.19	77.54	65.26	76.49	69.82	65.26	73.33	74.39
(#181 / #247) Tennis Court	**100**	**100**	**100**	**100**	**100**	**100**	**100**	**100**	**100**	**100**	**100**	**100**
(#187 / #473) Running Track	97.25	**100**	14.80	**100**	98.94	**100**	**100**	98.73	99.15	99.15	98.31	98.73

and $A_{ij}^{\mathrm{Ele}} = 1$. In this definition, all the connected nodes had the same weight on their edges, without accounting for actual differences in the spectral, spatial, and elevation proximities of different data point pairs. However, this may not be true in real cases. For example, it is more probable that a data point has similar characteristics with its nearest neighbors than with those points that are far apart. Therefore, in this letter, we propose a *generalized* fusion graph $\mathbf{G}^{\mathrm{GFus}} = (\mathbf{X}^{\mathrm{Sta}}, \mathbf{Q}^{\mathrm{GFus}})$. Suppose Δ is a pairwise distance matrix of the stacked features $\mathbf{X}^{\mathrm{Sta}}$. We propose a fused distance matrix as

$$\Delta^{\mathrm{GFus}} = \Delta + \mathbf{A}^{\mathrm{Neg}} \max(\Delta) \tag{3}$$

where $\mathbf{A}^{\mathrm{Neg}} = \neg\mathbf{A}^{\mathrm{Fus}}$, and the operator "$\neg$" denotes logical negation. Let $\mathcal{N}_i$ denote the k-NN of $\mathbf{x}_i$. For each node $\mathbf{x}_i$ ($i \in \{1, \ldots, n\}$), we first find its k-NN $\mathcal{N}_i$ in the fused distance matrix Δ^{GFus}. The edges are then formally defined as

$$Q_{ij}^{\mathrm{GFus}} = \begin{cases} e^{-\|\mathbf{x}_i - \mathbf{x}_j\|}, & \text{if } \mathbf{x}_j \in \mathcal{N}_i \\ 0, & \text{otherwise.} \end{cases} \tag{4}$$

Note that the edges denoted by $\mathbf{A}^{\mathrm{Fus}}$ or $\mathbf{A}^{\mathrm{Neg}}$ are still binary, whereas the edges of $\mathbf{Q}^{\mathrm{GFus}}$ are weighted with different values according to their distance if they are connected. The use of the neighborhood $\mathcal{N}_i$ in this equation guarantees that those data points that differ strongly in any of the spectral, spatial, or elevation characteristics will not be connected in the graph. For example, the data points from football fields made of real grass ($\mathbf{x}_i^{\mathrm{Sta}}$) and those made of synthetic grass ($\mathbf{x}_j^{\mathrm{Sta}}$) have very similar spatial and altitude information ($\mathbf{A}_{i,j}^{\mathrm{Spa}} = 1$, $\mathbf{A}_{i,j}^{\mathrm{Ele}} = 1$), but different spectral characteristics ($\mathbf{A}_{i,j}^{\mathrm{Spe}} = 0$). Then, $A_{i,j}^{\mathrm{Neg}} = 1$, and the distance $\Delta_{i,j}^{\mathrm{GFus}}$ in (3) will be penalized by adding the maximum value of Δ. Hence, the data points that are strongly dissimilar in any of the three characteristics are not likely to be within each other's k-NN, i.e., they are not likely to be connected in the fused graph. When using the constraint in [17] for avoiding degeneracy

$$\mathbf{W}^T(\mathbf{X}^{\mathrm{Sta}})\mathbf{D}^{\mathrm{GFus}}(\mathbf{X}^{\mathrm{Sta}})^T\mathbf{W} = \mathbf{I} \tag{5}$$

where $\mathbf{D}^{\mathrm{GFus}}$ is a diagonal matrix with $D_{i,i}^{\mathrm{GFus}} = \sum_{j=1}^{n} Q_{i,j}^{\mathrm{GFus}}$ and $\mathbf{I}$ is the identity matrix, we can obtain the transformation matrix $\mathbf{W} = (\mathbf{w}_1, \mathbf{w}_2, \ldots, \mathbf{w}_r)$, which is made up by r eigenvectors associated with the least r eigenvalues $\lambda_1 \leq \lambda_2 \leq \cdots \leq \lambda_r$ of the following generalized eigenvalue problem:

$$(\mathbf{X}^{\mathrm{Sta}})\mathbf{L}^{\mathrm{GFus}}(\mathbf{X}^{\mathrm{Sta}})^T\mathbf{w} = \lambda(\mathbf{X}^{\mathrm{Sta}})\mathbf{D}^{\mathrm{GFus}}(\mathbf{X}^{\mathrm{Sta}})^T\mathbf{w} \tag{6}$$

where $\mathbf{L}^{\mathrm{GFus}} = \mathbf{D}^{\mathrm{GFus}} - \mathbf{Q}^{\mathrm{GFus}}$ is the fusion Laplacian matrix.

IV. EXPERIMENTAL RESULTS

Experiments are done on an HSI and LiDAR data that were acquired by the NSF-funded Center for Airborne Laser Mapping (NCALM) on June 2012 over the University of Houston campus and the neighboring urban area. The HS imagery has 144 spectral bands with a wavelength range from 380 to 1050 nm. Both data sets have the same spatial resolution (2.5 m). The whole scene of the data, consisting of the full 349 $\times$ 1905 pixels, contains 15 classes. Available training and testing sets are given in Table I (# number of training samples/# number of test samples), and Fig. 2 shows the false color image of HS data and test samples. For more information, see [18].

The SVM classifier with radial basis function [19] kernels is applied in our experiments. The parameters of the SVM classifier are set the same as in our previous work [11]. Different feature sources are scaled to $[-1, 1]$ before classification. We compare our proposed GGF with the following schemes: 1) using the original HSI; 2) using the MPs computed on the first two PCs of the original HSI (MPs$_{\mathrm{HSI}}$); 3) using the MPs computed on the LiDAR data (MPs$_{\mathrm{LiDAR}}$); 4) stacking morphological features computed from both LiDAR data and the first two PCs of the original HSI (MPs$_{\mathrm{HSLi}}$), similarly as [6]; 5) stacking all dimensional normalized features, i.e., $\mathbf{X}^{\mathrm{Sta}}$ (Sta); 6) stacking all the features extracted by PCA from each individual feature, which represents more than 99% of the cumulative variance (PCA); 7) stacking all the features extracted by nonparametric weighted feature extraction (NWFE) [20] from each individual feature (which represents more than 99%

Fig. 2. Classification maps produced by the described schemes. (a) False color image with 15 classes labeled and highlighted in the image. Thematic maps using (b) MPs_{HSLi}, (c) LPP, (d) GFHL_{Org}, (e) GGF_{Org}, (f) GFHL [11], and (g) GGF.

of the cumulative variance); 8) features fused by using the graph constructed by all stacked feature sources (i.e., LPP [17]); and 9) our previous work with the edges of the fusion graph binary [11] (GFHL). Both GFHL and our proposed GGF can operate on all feature sources without and with KPCA normalization. We denote feature fusion on original feature sources without KPCA normalization as GFHL_{org} and GGF_{org}, respectively. In our experiments, 5000 samples were randomly selected to train KPCA, LPP, GFHL, and our proposed GGF.

The classification results are quantitatively evaluated by measuring the overall accuracy (OA), the average accuracy (AA), and the Kappa coefficient (κ) on the test samples. The experiments were carried out on a 64-bit 3.40-GHz Intel i7-4930K (1 core) CPU computer with 64-GB memory, and the consumed time includes normalization, feature fusion, and classification. Table I shows the accuracies and consumed time obtained from the experiments. For visual comparison, we show the classification maps in Fig. 2.

Form the table and figure, we have the following findings.

1) The results confirm that the fusion of the spectral, spatial, and elevation features can improve the classification performances. In particular, our proposed GGF produced the best OA, AA, and κ. The improvements of GGF in OA are 3.50%–12.93% compared with schemes 1–8. However, increasing the processing time with KPCA normalization, both GFHL and GGF have more than 3% improvements in κ compared with the GFHL_{org} and GGF_{org} without KPCA normalization. Compared with setting the edge of fusion graph binary (GFHL) in [11], the proposed generalized fusion graph (GGF) produces higher overall accuracies, particularly without KPCA normalization.
2) From the class-specific accuracies, when single features are used, the Raw_{HSI} approach produces better results on class "Tree," whereas MPs_{HSI} performs better on classes "Residential" and "Road," and the $\text{MPs}_{\text{LiDAR}}$ approach performs better on classes "Commercial" and "Highway." The proposed GGF produces higher accuracy on some classes related to nature resources, e.g., grass and tree. For some man-made objects such as "Commercial" and "Highway," both GFHL and GGF perform better than schemes 1–8.
3) From the classification maps, we can visually see that the objects under cloud regions are not well classified by using the stacked features. Without KPCA normalization, the proposed GGF_{org} classifies objects under cloud better than GFHL_{org}, with less consumed time.

The remote sensing data from the urban area was a mix between man-made structures and natural materials, and different objects may be made by same materials. It is difficult to classify them only using HS data, for example, some land-use classes (e.g., commercial and highway) are better classified when using LiDAR data. This is because commercial objects have larger area and higher elevation than residential objects and highway objects have higher elevation than road objects. By concentrating on different features in the stacked structure, the classification accuracies are improved. The approaches of NWFE and Sta are similar to the PCA approach in terms of a stacked architecture; all these three approaches first applied feature extraction on each individual feature and then concatenated the extracted feature vectors from the original HS data, the MPs of the HSI, and the MPs of LiDAR into one stacked vector. The differences are that each individual feature is represented by different aspects, e.g., the features extracted by PCA represent most of the cumulative variance in the data, whereas the features extracted by NWFE respect the class discriminant. The cloud-covered regions in the original HSI are not classified well by fusing features in a stacked architecture, because the elevation information contained in the

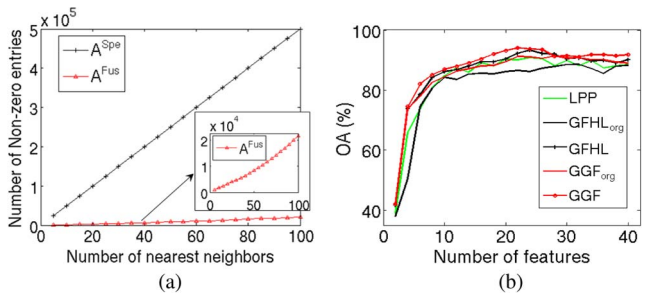

Fig. 3. (a) Number of nonzero entries in $\mathbf{A}^{\mathrm{Spe}}$ and $\mathbf{A}^{\mathrm{Fus}}$ as a function of the number of the nearest neighbors. (b) OA on the number of extracted features.

morphological features of LiDAR data is not well represented in such a way of data fusion. The spectral and spatial information $(\mathrm{MPs}_{\mathrm{HS}})$ of the cloud-covered regions is not related to real ground cover. The LiDAR sensor can penetrate clouds, and its morphological features contain the elevation information of the real ground cover. When stacking all feature sources together, the element values of different features can be significantly unbalanced, and the information contained by different feature sources is not equally represented. The same problems happen when using the stacked features to build a graph in the LPP method. By building the binary fusion graph, GFHL [11] cannot classify some objects under cloud well, particularly $\mathrm{GFHL}_{\mathrm{org}}$ without KPCA normalization. This is because both GFHL and $\mathrm{GFHL}_{\mathrm{org}}$ set all connected edges of the fusion graph to the same weight, which means that all connected points are treated as equally similar in terms of their characteristics. The proposed approach (GGF and $\mathrm{GGF}_{\mathrm{org}}$) assigns different weights to the connected edges according to a distance function and, in this way, better models the actual similarity of the connected nodes in their characteristics. Fig. 3(a) shows that there are fewer nonzero entries in $\mathbf{A}^{\mathrm{Fus}}$ than in $\mathbf{A}^{\mathrm{Spe}}$ (the number of nonzero entries is the same as $\mathbf{A}^{\mathrm{Spa}}$ and $\mathbf{A}^{\mathrm{Ele}}$) as the number of the nearest neighbors increases. With KPCA dimensional normalization, the OA of both GFHL and our proposed GGF are better than those without KPCA normalization (i.e., $\mathrm{GFHL}_{\mathrm{org}}$ and $\mathrm{GGF}_{\mathrm{org}}$) as the number of extracted features increases [see Fig. 3(b)].

V. Conclusion

The main contribution of this letter is a new methodology to include spectral, spatial, and elevation information in the classification process by a generalized graph-based feature fusion scheme. Compared with an older related method that used binary edges in the fusion graph, our new method, which employs weighted edges based on differences among spectral, spatial, and elevation features, better models the actual similarity of the connected nodes, which is reflected in improved classification performances.

Acknowledgment

The authors would like to thank the Hyperspectral Image Analysis Group and NCALM at the University of Houston for providing the data sets used in this study, as well as the IEEE GRSS Data Fusion Technical Committee for organizing the 2013 Data Fusion Contest.

References

[1] E. Simental, D. J. Ragsdale, E. Bosch, R. Dodge, Jr., and R. Pazak, "Hyperspectral dimension reduction and elevation data for supervised image classification," in *Proc. 14th ASPRS Conf*, Anchorage, AK, USA, May 3–9, 2003.

[2] D. Lemp and U. Weidner, "Improvements of roof surface classification using hyperspectral and laser scanning data," in *Proc. ISPRS Joint Conf.—3rd Int. Symp. Remote Sens. Data Fusion Over URBAN Areas/5th Int. Symp. URS Areas*, Tempe, AZ, USA, Mar 14–16, 2005.

[3] B. Koetz *et al.*, "Fusion of imaging spectrometer and LIDAR data over combined radiative transfer models for forest canopy characterization," *Remote Sens. Environ.*, vol. 106, no. 4, pp. 449–459, Feb. 2007.

[4] X. Huang, L. Zhang, and W. Gong, "Information fusion of aerial images and LIDAR data in urban areas: Vector-stacking, re-classification and post-processing approaches," *Int. J. Remote Sens.*, vol. 32, no. 1, pp. 69–84, Jan. 2011.

[5] M. Dalponte, L. Bruzzone, and D. Gianelle, "Fusion of hyperspectral and LIDAR remote sensing data for classification of complex forest areas," *IEEE Trans. Geosci. Remote Sens.*, vol. 46, no. 5, pp. 1416–1427, May 2008.

[6] M. Pedergnana, P. R. Marpu, M. D. Mura, J. A. Benediktsson, and L. Bruzzone, "Classification of remote sensing optical and LiDAR data using extended attribute profiles," *IEEE J. Sel. Topics Signal Process.*, vol. 6, no. 7, pp. 856–865, Nov. 2012.

[7] L. Zhang, L. Zhang, D. Tao, and X. Huang, "On combining multiple features for hyperspectral remote sensing image classification," *IEEE Trans. Geosci. Remote Sens.*, vol. 50, no. 3, pp. 879–893, Mar. 2012.

[8] X. Huang and L. Zhang, "An SVM ensemble approach combining spectral, structural, semantic features for the classification of high-resolution remotely sensed imagery," *IEEE Trans. Geosci. Remote Sens.*, vol. 51, no. 1, pp. 257–272, Jan. 2013.

[9] M. D. Mura, J. A. Benediktsson, B. Waske, and L. Bruzzone, "Extended profiles with morphological attribute filters for the analysis of hyperspectral data," *Int. J. Remote Sens.*, vol. 31, no. 22, pp. 5975–5991, Nov. 2010.

[10] M. D. Mura, A. Villa, J. A. Benediktsson, J. Chanussot, and L. Bruzzone, "Classification of hyperspectral images by using extended morphological attribute profiles and independent component analysis," *IEEE Geosci. Remote Sens. Lett.*, vol. 8, no. 3, pp. 541–545, May 2011.

[11] C. Debes *et al.*, "Hyperspectral and LiDAR data fusion: Outcome of the 2013 GRSS Data Fusion Contest," *IEEE J. Sel. Topics Appl. Earth Observ. Remote Sens.*, vol. 7, no. 6, pp. 2405–2418, Jun. 2014.

[12] W. Liao, R. Bellens, A. Pižurica, W. Philips, and Y. Pi, "Classification of hyperspectral data over urban areas using directional morphological profiles and semi-supervised feature extraction," *IEEE J. Sel. Topics Appl. Earth Observ. Remote Sens.*, vol. 5, no. 4, pp. 1177–1190, Aug. 2012.

[13] R. Bellens *et al.*, "Improved classification of VHR images of urban areas using directional morphological profiles," *IEEE Trans. Geosci. Remote Sens.*, vol. 46, no. 10, pp. 2803–2812, Oct. 2008.

[14] W. Liao, R. Bellens, A. Pižurica, W. Philips, and Y. Pi, "Classification of hyperspectral data over urban areas based on extended morphological profile with partial reconstruction," in *Proc. ACIVS*, Brno, Czech Republic, 2012, pp. 278–289.

[15] B. Scholkopf, A. J. Smola, and K. R. Muller, "Nonlinear component analysis as a kernel eigenvalue problem," *Neural Comput.*, vol. 10, no. 5, pp. 1299–1319, Jul. 1998.

[16] M. Belkin and P. Niyogi, "Laplacian eigenmaps and spectral techniques for embedding and clustering," in *Advances in Neural Information Processing Systems 14*. Cambridge, MA, USA: MIT Press, 2001, pp. 585–591.

[17] X. F. He and P. Niyogi, "Locality preserving projections," in *Advances in Neural Information Processing Systems 16*. Cambridge, MA, USA: MIT Press, 2004, pp. 153–160.

[18] IEEE GRSS Data Fusion Contest 2013. [Online]. Available: http://www.grss-ieee.org/community/technical-committees/data-fusion/

[19] C. C. Chang and C. J. Lin, LIBSVM: A Library for Support Vector Machines, 2001. [Online]. Available: http://www.csie.ntu.edu.tw/~cjlin/libsvm

[20] B. C. Kuo and D. A. Landgrebe, "Nonparametric weighted feature extraction for classification," *IEEE Trans. Geosci. Remote Sens.*, vol. 42, no. 5, pp. 1096–1105, May 2004.

[21] M. Fauvel, J. A. Benediktsson, J. Chanussot, and J. R. Sveinsson, "Spectral and spatial classification of hyperspectral data using SVMs and morphological profile," *IEEE Trans. Geosci. Remote Sens.*, vol. 46, no. 11, pp. 3804–3814, Nov. 2008.